Published in final edited form as:
Cancer Cell. 2014 December 8; 26(6): 863–879. doi:10.1016/j.ccell.2014.10.010.

Copy Number Gain of hsa-miR-569 at 3q26.2 Leads to Loss of TP53INP1 and Aggressiveness of Epithelial Cancers

Pradeep Chaluvally-Raghavan[1,*], **Fan Zhang**[1], **Sunila Pradeep**[2,3], **Mark P. Hamilton**[11], **Xi Zhao**[12,13], **Rajesha Rupaimoole**[2,3], **Tyler Moss**[1], **Yiling Lu**[1], **Shuangxing Yu**[1], **Chad V. Pecot**[4,18], **Miriam R. Aure**[12,13], **Sylvain Peuget**[14,15,16], **Cristian Rodriguez-Aguayo**[5], **Hee-Dong Han**[2,3], **Dong Zhang**[1], **Avinashnarayan Venkatanarayan**[6], **Marit Krohn**[12,13], **Vessela N. Kristensen**[12,13], **Mihai Gagea**[7], **Prahlad Ram**[1], **Wenbin Liu**[8], **Gabriel Lopez-Berestein**[5,10], **Philip L. Lorenzi**[8], **Anne-Lise Børresen-Dale**[12,13], **Koei Chin**[17], **Joe Gray**[15], **Nelson J. Dusetti**[14,15,16], **Sean E. McGuire**[9,11], **Elsa R. Flores**[6], **Anil K. Sood**[2,3,10], and **Gordon B. Mills**[1,*]

[1]Department of Systems Biology, The University of Texas MD Anderson Cancer Center, Houston, TX 77054, USA

[2]Department of Gynecologic Oncology, The University of Texas MD Anderson Cancer Center, Houston, TX 77054, USA

[3]Department of Cancer Biology, The University of Texas MD Anderson Cancer Center, Houston, TX 77054, USA

[4]Department of Thoracic, Head and Neck Oncology, The University of Texas MD Anderson Cancer Center, Houston, TX 77054, USA

[5]Department of Experimental Therapeutics, The University of Texas MD Anderson Cancer Center, Houston, TX 77054, USA

[6]Department of Biochemistry and Molecular Biology, The University of Texas MD Anderson Cancer Center, Houston, TX 77054, USA

[*]Correspondence: pcraghavan@mdanderson.org (P.C.-R.), gmills@mdanderson.org (G.B.M.), http://dx.doi.org/10.1016/j.ccell.2014.10.010.

[18]Present address: Department of Molecular Therapeutics, UNC Lineberger Comprehensive Cancer Center, School of Medicine, Chapel Hill, NC 27599, USA

SUPPLEMENTAL INFORMATION

Supplemental Information includes Supplemental Experimental Procedures, seven figures, and four tables and can be found with this article online at http://dx.doi.org/10.1016/j.ccell.2014.10.010.

AUTHOR CONTRIBUTIONS

G.B.M. and P.C.R. conceived the study, generated hypotheses and designed experiments. P.C.R. performed most experiments including tissue culture, animal experiments, immunofluorescence and 3D morphogenesis. FZ, WL, X.Z., M.R.A., M.K., and V.N.K. performed bioinformatics analysis. G.B.M. and A.-L.B.-D. supervised the bioinformatics analysis. P.C.R., C.V.P., S.P., and A.K.S. designed the in vivo antimiR experiments. S.P. performed IHC experiments, assisted in animal experiments and in vivo delivery of antimiR. S.Y. prepared miR569 stable cells and performed mutagenesis on the TP53INP1 3′UTR. A.V. and E.R.F. provided TP53 and TP73 KO cells. S. Peuget and N.J.D. provided TP53INP1 KO cells. Y.L., S.Y., and D.Z. performed RPPA analysis. R.R., H.-D.H., C.-R.A., G.L.-B. and A.K.S. incorporated antimiR in nanoliposomes for in vivo experiments. D.Z. provided technical assistance for all animal experiments. P.L.L. performed isobologram analysis. K.C. and J.G. assisted with analysis of effects of copy number on expression of miR569 and its targets. T.M. and P.R. performed Netwalker analysis. M.H. and SMG performed AGO-CLIP data analysis. MG analyzed histopathology slides. G.B.M. provided scientific direction, established collaborations, prepared the manuscript with P.C.R. and allocated funding for the work.

[7]Department of Veterinary Medicine and Surgery, The University of Texas MD Anderson Cancer Center, Houston, TX 77054, USA

[8]Department of Bioinformatics and Computational Biology, The University of Texas MD Anderson Cancer Center, Houston, TX 77054, USA

[9]Department of Radiation Oncology, The University of Texas MD Anderson Cancer Center, Houston, TX 77054, USA

[10]Center for RNAi and Non-Coding RNA, The University of Texas MD Anderson Cancer Center, Houston, TX 77054, USA

[11]Department of Molecular and Cellular Biology, Baylor College of Medicine, Houston, TX 77030, USA

[12]Department of Genetics, Institute for Cancer Research, Oslo University Hospital, the Norwegian Radium Hospital, 0424 Oslo, Norway

[13]The K.G. Jebsen Center for Breast Cancer Research, Institute for Clinical Medicine, Faculty of Medicine, University of Oslo, 0424 Oslo, Norway

[14]INSERM U1068, CRCM, Cell Stress, Marseille F-13009, France

[15]Institut Paoli-Calmettes, 13273 Marseille Cedex 9, France

[16]UMR7258, CNRS, Aix-Marseille University, Marseille F-13009, France

[17]Department of Biomedical Engineering, School of Medicine, Oregon Health and Science University, Portland, OR 97239, USA

SUMMARY

Small noncoding miRNAs represent underexplored targets of genomic aberrations and emerging therapeutic targets. The 3q26.2 amplicon is among the most frequent genomic aberrations in multiple cancer lineages including ovarian and breast cancers. We demonstrate that hsa-miR-569 (hereafter designated as miR569), which is overexpressed in a subset of ovarian and breast cancers, at least in part due to the 3q26.2 amplicon, alters cell survival and proliferation. Downregulation of *TP53INP1* expression by miR569 is required for the effects of miR569 on survival and proliferation. Targeting miR569 sensitizes ovarian and breast cancer cells overexpressing miR569 to cisplatin by increasing cell death both in vitro and in vivo. Thus targeting miR569 could potentially benefit patients with the 3q26.2 amplicon and subsequent miR569 elevation.

INTRODUCTION

Genomic instability, including DNA copy number aberrations (CNAs), is a hallmark of cancer. Noncoding genes represent potential targets of CNAs and cancer drivers (Esquela-Kerscher and Slack, 2006). Thus, characterization of altered miRNA resulting from CNAs could improve our understanding of tumor initiation and progression as well as provide molecular markers for early detection, prognosis and response prediction, and targets for therapy. Both high-grade serous ovarian cancer and basal-like breast cancer, the most

aggressive forms of ovarian and breast cancers, appear to be driven by CNAs (Cancer Genome Atlas Research Network, 2011, 2012; Ciriello et al., 2013). Amplification of chromosome 3q26.2 is a common event in ovarian (Eder et al., 2005) and breast cancers (Weber-Mangal et al., 2003). The 3q26.2 amplicon is large and structurally complex consistent with multiple components of the amplicon contributing to tumor initiation and progression either alone or through cooperative activity. We have demonstrated that the 3q26.2 CNA leads to amplification and aberrant function of *PIK3CA*, *PKCI*, *SKIL*, and *MECOM* (Eder et al., 2005; Nanjundan et al., 2008).

RESULTS

Amplification of 3q26.2 Is Associated with Increased Expression of miR569

To better define aberration within the 3q26 region, we used high-resolution SNP-based copy number analysis of 533 high-grade serous epithelial ovarian cancers and 841 breast cancers from The Cancer Genome Atlas (TCGA). At least one copy of 3q26.2 was gained in approximately 35% of high-grade serous epithelial ovarian cancers (Figure 1A) and 15% of breast cancers (Figures S1A and S1B available online). In addition to expression of genes located at 3q26.2 being increased, our results demonstrate that miR569 expression was increased as a consequence of the 3q26.2 amplicon. Quantitative real-time PCR (qRT-PCR) analysis of 33 ovarian cancer samples demonstrated a marked increase in mature miR569 in 18/24 tumors with the 3q26.2 amplicon (more than four copies), relative to 0/9 nonamplified tumors (Figure 1B; Figure S1C). The association of mature miR569 levels with 3q26.2 amplification (more than three copies) was confirmed in ovary and breast epithelial cell lines including immortalized normal cell lines (Figures 1C and 1D). Importantly, miR569 was highly expressed in ovarian cancers compared to normal ovary or fallopian tube (Figure 1E). Thus, miR569 expression is likely dysregulated as a consequence of the 3q26.2 amplicon. However, additional mechanisms may be involved in the regulation of miR569 levels because not all tumors with the 3q26.2 amplicon have elevated miR569.

To identify regulators of miR569, mRNAs most positively correlated with miR569 in a public data set (Bentink et al., 2012) were used to develop a gene protein interaction map in the Netwalker gene network analysis suite (Komurov et al., 2012) (Table S1; Figure S1D). Among 11 candidate mediators, target-specific knockdown of NF-κB2 and SPHK1 decreased miR569 levels (Figures S1E–S1G). Analysis using CHIPBASE (Yang et al., 2013) was consistent with NF-κB regulating miR569 expression (Figure S1H). Compatible with a previous report (Liang et al., 2013), we propose that the SPHK1-NF-κB axis (Figure S1I) and copy number changes of miR569 regulate miR569 levels.

miR569 Alters Cell Proliferation and Viability of Breast and Ovarian Cell Lines

Enforced expression of miR569 in the immortalized ovarian epithelial cell line IOSE-80 and mammary epithelial cell line MCF10A, which do not have 3q26.2 amplification and exhibit low miR569 levels (Figure 1C), increased cell proliferation in 2D cultures (Figure 1F; Figure S1J) and increased the number and size of spheroids in 3D cultures (Figures 1G and 1H; Figures S1K and S1L). Importantly, MCF10A stably expressing miR569 demonstrated luminal filling with less caspase-3 activation as compared to control cells (Figures S1L and

S1M). In parallel, knockdown with anti-miR569 in HEYA8 and OVCAR5 ovarian cancer cells, which have the 3q26.2 amplicon and elevated miR569 levels (Figure 1C), increased cleaved PARP and cleaved caspase 3 (Figure 1I). Furthermore, anti-miR569 reduced the G2 population and increased the G1 population (Figure S1N) concomitant with a marked increase in a sub G0/G1 population (Figure S1O) and cell death (Figure S1P). The effect of anti-miR569 on apoptosis was confirmed using a cell death-specific ELISA kit (Figure 1J; Figure S1Q). Furthermore, a pan-caspase inhibitor abolished anti-miR569 induced cell death (Figure 1J). Altogether, our results suggest that miR569 promotes cell proliferation and inhibits apoptosis.

miR569 Expression Promotes Tumor Growth and Metastasis In Vivo

To determine whether miR569 alters tumor growth in vivo, 3q26.2 nonamplified IGROV1 ovarian cancer cells (Figure 2A) or MDAMB231 breast cancer cells (Figure 2B) stably overexpressing miR569 or control miR were injected orthotopicallly into the peritoneal cavity or mammary fat pad of nude mice, respectively. Enforced expression of miR569 in both breast and ovarian cancer cells significantly increased tumor growth and tumor weight (Figures 2C–2F; Figures S2A and S2B). Ki67 and CD31 levels were significantly elevated in miR569-expressing IGROV1 and MDAMB231 tumors compatible with increases in cell proliferation and angiogenesis (Figures 2G and 2H; Figures S2C and S2D). Strikingly, the number of peritoneal implants as well as lung metastases (Figure 2I) were increased in mice with miR569-expressing IGROV1 tumors and lung metastases were increased in mice with miR569-expressing MDAMB231 tumors (Figures 2J and 2K). Thus, expression of miR569 in breast and ovarian cancer cells lacking the 3q26.2 amplicon is sufficient to increase tumor growth, proliferation, neovascularization, and metastatic capability.

TP53INP1 Is a Direct Target of miR569

To identify targets of miR569 that could alter cell survival, we used an integrative approach combining microRNA target predictions from TargetScan (Lewis et al., 2005) (Table S2) and publicly available human Argonaute crosslinking immunoprecipitation (AGO-CLIP) data (Chi et al., 2009; Hafner et al., 2010) that ranks the relative confidence of miRNA targets by their presence in 14 AGO-CLIP libraries (Hamilton et al., 2013). miR569 targets detected in ≥5 of 14 AGO-CLIP data sets were considered high confidence candidates ($q < 0.001$ based on random permutation of clusters) (Table S3). High confidence AGO-CLIP targets were overlaid with putative TargetScan miR569 targets resulting in 17 common targets (Table S4; Figure 3A). Of the 17 candidates assessed, miR569 markedly decreased *TP53INP1* mRNA levels in IOSE-80 ovarian epithelial cells (Figure 3B) consistent with *TP53INP1* being a miR569 target. miR569 binding to the 3′UTR of *TP53INP1* was identified in six of 14 independent AGO-CLIP data sets (Figure 3C). Furthermore, miR569 decreased TP53INP1 protein levels in normal breast and ovarian cells (Figure 3D), whereas anti-miR569 increased TP53INP1 levels in HEYA8 and OVCAR5 cells that have high miR569 levels (Figure 3E). Importantly, 3q26.2 amplification status and miR569 levels (Figure 1C) were inversely correlated with TP53INP1 protein levels in cell lines (Figure 4A), consistent with the contention that miR569 silences *TP53INP1* expression. Furthermore, tumors that arose from cells engineered to express miR569 (Figure 2) had decreased *TP53INP1* levels (Figure S3A), again supporting *TP53INP1* as a miR569 target.

TargetScan predicted a single miR569 binding site in the *TP53INP1* 3′UTR (Figure S3B). Compatible with miR569 directly binding to the *TP53INP1* 3′UTR, miR569 markedly decreased the activity of luciferase fused to the *TP53INP1* 3′UTR in both breast and ovarian cancer cells (Figure 4B). In contrast, miR569 expression did not alter activity of luciferase linked to a *TP53INP1* 3′UTR where the putative miR569 binding site was mutated (Figures S3C and S3D).

TP53INP1 Is Required for miR569 to Alter Cell Proliferation and Viability

Although miR569 is not annotated in the mouse genome, sequences complementary to miR569 seed sequences are present in the murine *Tp53inp1* 3′UTR (Figure S3E). Importantly, miR569 increased proliferation of wild-type (WT) mouse embryonic fibroblasts (MEFs) but not *Tp53inp1*-deficient MEFs (Figures 4C and 4D; Figure S3F). Furthermore, miR569 expression reduced *Tp53inp1* mRNA and TP53INP1 protein levels in WT MEFs (Figures 4E and 4F). Because miR569 is not expressed in mouse, we determined whether TP53INP1 is required for the effects of anti-miR569 in human cells. Anti-miR569 did not alter TP53INP1 expression or cell death in murine cells (Figures S3G–S3I) consistent with the effects of anti-miR569 being specific to miR569. In contrast, knockdown of TP53INP1 abolished the effects of anti-miR569 on cell death in miR569-expressing human cells (Figures S3J–S3L). Importantly, miR569 reduced the activity of p53 as well as the promoter activity of the p53 target gene *PERP* in WT MEFs and HEYA8, but not in *Tp53inp1*$^{-/-}$ MEFs (Figures S3M and S3N). Together, these results support that TP53INP1 is required for the effects of miR569.

Next, we used 3D cultures on extracellular matrix to mimic in vivo conditions. In 3D culture, MCF10A breast and MCAS ovarian epithelial cells evolve into ~150 μm single-layered acinar structures with a hollow lumen through death of luminal cells (Muranen et al., 2012; Pradeep et al., 2012a). Strikingly miR569-transfected breast and ovarian epithelial spheroids had decreased *TP53INP1* expression and generated multilayered cell structures consistent with decreased death of cells in the lumen (Figures 4G–4I; Figures S3O–S3Q). Of note, siRNA-mediated knockdown of *TP53INP1* in MCAS spheroids was sufficient to mimic the effects of miR569 with a marked increase in the number of multilayered spheroids (Figures S3R–S3T), reinforcing the contention that *TP53INP1* is a key target of miR569.

The effects of miR569 in 3D culture suggested that miR569 could alter self-renewal or tumor-initiating capacity (TIC). Indeed, miR569 altered levels of markers associated with TICs including increased *CD44*, *CD133*, and *VIM* (vimentin) and decreased *CDH1* (E-cadherin) in MCAS cells and increased *CD44* and *VIM* and decreased *CDH1* in MCF10A cells. Whereas miR569 increased the number of MCAS spheroids in 3D culture, it was sufficient to increase the self-renewal capacity of MCF10A cells in serial passages (Figures 4J and 4K; Figures S3U and S3V), consistent with a role in TIC in MCF10A cells.

TP53INP1 Expression Is Regulated by p53, p73, and NF-κB

Although p53 is the major transcriptional regulator of *TP53INP1* (Okamura et al., 2001; Tomasini et al., 2001), *TP53INP1* can also be regulated by p73 in a p53-independent manner

(Tomasini et al., 2005). *TP53* is almost universally mutated in high-grade serous ovarian cancers but less frequently mutated in breast cancers (Cancer Genome Atlas Research Network, 2012; Gasco et al., 2002; Greenblatt et al., 1994). Importantly, *TP53INP1* levels were decreased in *TP53*-mutated breast cancers in four different patient data sets (n = 757, Figures S4A and 7I). In addition to p53 and p73 binding sites, there are consensus NF-κB and N-Myc binding sequences in the *TP53INP1* promoter (Figure S4B). In IOSE-80, knockdown of p53 or p73 reduced *TP53INP1* expression, whereas knockdown of NF-κB1 or N-Myc had no effect (Figure 5A). Cotransfection of miR569 with either p53 or p73 siRNA decreased TP53INP1 levels consistent with miR569 regulating *TP53INP1* induced by p53 or p73 (Figure 5B). Importantly, knockdown of either p53 or p73 increased cell growth moderately, with coordinate knockdown of p53 and p73 further enhancing IOSE-80 cell proliferation (Figures 5B and 5C). Moreover, cotransfection of miR569 with p53 siRNA or p73 siRNA increased growth of IOSE-80 cells to levels comparable to concurrent knockdown of p53 and p73. Importantly, miR569 did not further increase cell growth with concurrent p53 and p73 knockdown (Figures 5B and 5C) likely due to cells with concurrent p53 and p73 knockdown having insufficient *TP53INP1* to manifest the effects of miR569. These results were recapitulated in *Trp53*$^{-/-}$ or *Trp73*$^{-/-}$ MEFs, where deletion of either *Trp53* or *Trp73* reduced expression of *Tp53inp1* mRNA, whereas double knock-out *Trp53*$^{-/-}$*;Trp73*$^{-/-}$ MEFs (Flores et al., 2002) expressed the lowest amounts of *Tp53inp1* (Figure 5D). Similarly, transfection of miR569 increased proliferation of *Trp53*$^{-/-}$ or *Trp73*$^{-/-}$ MEFs but not double knockout MEFs (Figure 5E).

In HEYA8 cells, which express WT p53 (Figures S4C and S4D), knockdown of p53, p73, or NF-κB decreased *TP53INP1* expression (Figure 5F). In OVCAR5, CaOV3, or SKOV3 p53 mutant ovarian cancer cell lines, knockdown of p73 or NF-κB1 but not p53 decreased expression of *TP53INP1* (Figure 5G; Figure S4E). Thus p53, or p73 and other transcription factors including NF-κB or possibly N-Myc, albeit not in the cells assessed herein, can contribute to transcriptional regulation of *TP53INP1* under different contexts, which is further downregulated by miR569.

Silencing of miR569 Sensitizes Cells to Chemotherapy-Induced Cell Death

We next determined whether miR569 alters sensitivity to cisplatin, the most commonly used drug in ovarian cancer and an emerging therapy for basal-like breast carcinoma. Of note, miR569 expression reduced the sensitivity of normal breast and ovarian epithelial cells to cisplatin (Figure 6A). Isobologram analysis showed synergistic activity of the anti-miR569 and cisplatin combination (Figure S5A). In HEYA8 (Figure 6B; Figure S5B) and OVCAR5 (Figure S5C) that have detectable TP53INP1 basal levels, cisplatin alone increased TP53INP1, which was augmented by anti-miR569. TP53INP1 can induce phosphorylation of p53Ser46, which contributes to stress-induced apoptosis in cancer cells (Okamura et al., 2001; Tomasini et al., 2003). As expected, both cisplatin and knockdown of miR569 increased p53Ser46 phosphorylation, cleaved caspase-3 and PARP, and cell death, which increased further with the combination of cisplatin and anti-miR569 (Figure 6B; Figures S5C and S5D). Furthermore, anti-miR569 induced increases in p53Ser46 phosphorylation were paralleled by increases in total p53, PUMA, Bax, P53AIP1, and p21 proteins that regulate apoptosis and the cell cycle (Figure 6B).

As predicted, anti-miR569 modestly decreased cell survival and sensitized HEYA8 to cisplatin-induced apoptosis in both anchorage dependent and independent conditions (Figure 6C; Figures S5E and S5F). Notably, knockdown of TP53INP1, P53AIP1, and PUMA, but not NOXA, decreased anti-miR569-induced caspase activity and cell death and concurrently increased sphere forming ability of ovarian cancer cells (Figures S5G–S5J) while decreasing miR569-induced sensitization to cisplatin (Figures 6D and 6E). Importantly, knockdown of TP53INP1 completely reversed cell death and caspase activity induced by anti-miR569, while siRNA specific to PUMA or P53AIP1 partially reduced cell death induced by anti-miR569, consistent with TP53INP1 being a direct target of miR569 and with P53AIP1 and PUMA acting downstream of TP53INP1 (Figure S5I). To further assess the specificity of anti-miR569, HEYA8 stably expressing miR569 or control miR were transfected with control anti-miR or anti-miR569 and were treated with cisplatin. Strikingly, stable expression of miR569 markedly attenuated cisplatin-induced increases in TP53INP1, phosphorylated p53Ser46, p53, and PUMA, and increased colony formation, which were only partially reversed by anti-miR569 (Figures S5K–S5M). Thus, overexpression of miR569 is able to at least partially reverse effects of anti-miR569 consistent with the effects of anti-miR569 being on target.

Consistent with activation of caspase-3 and increased cell death, anti-miR569 and cisplatin induced cytochrome C release from mitochondria (Figure 6F; Figure S5N). Furthermore, anti-miR569 combined with cisplatin augmented cytochrome C release compared to each agent alone (Figure S5N). Cytochrome C release induced by anti-miR569 was inhibited by knockdown of p53AIP1 or TP53INP1, compatible with P53AIP1 or TP53INP1 being required for optimal anti-miR569-induced apoptosis (Figure 6F; Figure S5O). Together, the data support a model wherein gain of 3q26.2 copy number increases miR569 levels that in turn decrease TP53INP1 (Figure 6G) limiting the ability of stress, including chemotherapy-induced stress, to activate p53, p73, or NF-κB and induce proapoptotic proteins such as Bax, P53AIP1, and PUMA with subsequent cleavage of caspase-3 and PARP.

miR569 Copy Number Changes and *TP53INP1* Expression Are Associated with Ovarian and Breast Cancer Outcomes

Because *TP53INP1* is required for the effects of miR569, we determined whether TP53INP1 levels correlate with patient outcomes. Indeed, decreased *TP53INP1* mRNA levels were associated with worsened outcome (Figure 7A) in ovarian cancer (Tothill et al., 2008). Immunohistochemical analysis confirmed association of TP53INP1 levels with worsened patient outcomes (Figure 7B) and reduced TP53INP1 protein in ovarian cancer cells compared to normal epithelial cells (Figure 7C). Importantly, *TP53INP1* mRNA expression was markedly reduced in ovarian cancer samples that have high miR569 levels (Figure 7D). Furthermore, reduced *TP53INP1* expression was observed in invasive ovarian cancers compared to low malignant potential tumors (Figure S6A) and miR569 levels were increased in late compared to early stage ovarian cancers (Bagnoli et al., 2011) (Figure S6B).

In breast cancer samples, 3q26.2 copy number gain also associated with decreased *TP53INP1* mRNA levels (Figure 7E). Furthermore, gain of miR569 copy number as well as

decreased *TP53INP1* mRNA levels were significantly more common in basal-like breast cancers than in other breast cancer subtypes (Figures S6C–S6E). Similar to ovarian cancer, elevated miR569 copy number (Figure 7F) and decreased TP53INP1 protein levels (Figure 7G) were associated with worsened outcome in breast cancer. In an independent cohort of breast cancers (Pawitan et al., 2005) and a merged data set from three independent breast cancer cohorts (Enerly et al., 2011; Haakensen et al., 2010; Langerød et al., 2007; Muggerud et al., 2010; Naume et al., 2007), low *TP53INP1* mRNA levels were associated with worsened outcomes (Figure 7H; Figure S6F).

The almost universal mutation of *TP53* in high-grade serous ovarian cancer precluded exploration of the role of *TP53* mutation in regulating expression of *TP53INP1* or whether *TP53* mutation alters effects of the *TP53INP1* on ovarian cancer outcomes. However, as predicted by the role for p53 in regulation of *TP53INP1*, *TP53*-mutated breast cancer samples demonstrated lower *TP53INP1* mRNA and protein levels in the TCGA breast cancer data set and mRNA levels in three independent breast cancer cohorts (Enerly et al., 2011; Haakensen et al., 2010; Langerød et al., 2007; Muggerud et al., 2010; Naume et al., 2007) (Figure 7I; Figure S4A). Tumors with increased miR569 copy number and mutated *TP53* had lower *TP53INP1* mRNA levels, suggesting that the two events collaborate to decrease *TP53INP1* (Figures 7I and 7J; Figures S6G–S6I). miR569 copy number gain was associated with a poor outcome in patients with WT *TP53* (Figure 7K) and showed a trend to association with poor overall outcome in patients with mutant p53 (Figure S6J). This is consistent with mutant p53 or miR569 amplification decreasing *TP53INP1* levels.

We explored whether p53 was required for effects of *TP53INP1* on patient outcomes in breast cancers, where only a subset of tumors have *TP53* mutations. Strikingly, in 75 *TP53* mutant breast cancers from three independent cohorts (Haakensen et al., 2010; Langerød et al., 2007; Muggerud et al., 2010; Naume et al., 2007), *TP53INP1* levels predicted patient outcomes (Figure S6K). For reasons that are not clear, but potentially due to short-term follow-up of TCGA samples, the effects of *TP53INP1* on outcomes of patients with WT *TP53* in TCGA breast cancer data set showed a trend to poor outcomes with no association with outcomes in other cohorts assessed (Haakensen et al., 2010; Langerød et al., 2007; Muggerud et al., 2010) (data not shown). In breast cancer, WT *TP53* was associated with improved survival when five previously published breast cancer data sets were combined (Figure S6L). Intriguingly patients with tumors having both WT *TP53* and high *TP53INP1* levels showed remarkably improved breast cancer specific survival particularly in comparison to patients with low *TP53INP1* and mutant *TP53* (Figure S6M).

Silencing of miR569 Inhibits Tumor Growth and Metastasis in an Orthotopic Ovarian Cancer Model

To explore whether miR569 represents a potential therapeutic target, we incorporated anti-miR569 into neutral liposomes (1,2-dioleoyl-*sn*-glycero-3-phosphotidylcholine-DOPC) (Landen et al., 2005) and treated HEYA8 or OVCAR5 cells, which endogenously express miR569, orthotopic xenografts with and without cisplatin. Both anti-miR569 and cisplatin decreased tumor growth. Remarkably, the combination of anti-miR569 and cisplatin induced a massive decrease in tumor weight and number of tumor sites in the peritoneal cavity

(Figures 8A and 8B; Figure S7A). Consistent with in vitro studies (Figure 6), anti-miR569 treatment significantly reduced miR569 levels and increased both *TP53INP1* and *P53AIP1* mRNA levels. Cisplatin treatment moderately increased *TP53INP1* mRNA and *P53AIP1* mRNA as well as TUNEL staining as a marker of cell death. Noticeably, combined treatment with anti-miR569 and cisplatin further increased *TP53INP1* and *P53AIP1* mRNA expression and TUNEL positivity (Figures 8C–8F; Figures S7B and S7C). Anti-miR569 and cisplatin alone decreased levels of Ki67 proliferation and CD31 endothelial cell markers whereas combined treatment with anti-miR569 and cisplatin further reduced Ki67 and CD31 (Figures 8E and 8F; Figure S7B).

Similar to the effects on ovarian cancer models, anti-miR569 treatment reduced volume and weight of tumors derived from MDAMB231 that express high levels of miR569 (Figures S7D–S7G). Of note, liposomal delivery of anti-miR569 did not induce apoptosis or reduce tumor burden or metastasis when injected in mice bearing IGROV1 that do not have an elevated miR569 copy number (Figures S7H and S7I).

TP53INP1 Is Sufficient and Necessary for the Effects of Anti-miR569

Our data suggest that the effects of miR569 are dependent on the ability to alter *TP53INP1* levels. To test this contention in vivo, we determined the effect of altering *TP53INP1* levels on intraperitoneal HEYA8 growth. As predicted, expression of *TP53INP1* in HEYA8 decreased both number and size of tumors, recapitulating the effects of anti-miR569 in vivo (Figures S7J–S7L). In contrast, transient or stable knockdown of *TP53INP1* abolished the ability of anti-miR569 to decrease cell growth in vitro (Figures S5G, S7M, and S7N) and abolished the ability of anti-miR569 to decrease HEYA8 growth in vivo (Figures 8G and 8H). Taken together, the results show that TP53INP1 is a key target of miR569 both in vitro and in vivo.

DISCUSSION

Our studies demonstrate that copy number alterations of the 3q26.2 amplicon are associated with increased miR569 expression in ovarian and breast cancers. The increase in miR569 levels subsequently decreases *TP53INP1* levels. Through down-regulation of *TP53INP1*, miR569 increases cell proliferation, anchorage-dependent and -independent cell growth, allows the formation of multilamellar cellules, and increases tumor growth and metastasis in vivo. Intriguingly, anchorage-independent growth and ability to maintain cell survival in multilamellar cellules require a coordinate decrease in apoptosis and improved metabolic performance (Schafer et al., 2009). Thus, miR569 may affect both processes required for survival under anchorage-independent conditions. Consistent with these results, expression of *TP53INP1* in the tumorigenic MiaPaCa2 pancreatic cancer cell line abolished tumor-forming ability in nude mice through induction of caspase-3-mediated apoptosis (Gironella et al., 2007), and mice deficient in *Tp53inp1* were susceptible to colitis-associated carcinogenesis (Gommeaux et al., 2007).

The observation that miR569 was elevated as a consequence of the 3q26.2 amplicon and associated with decreased *TP53INP1* in ovarian cancer raised a number of questions given that p53 transcriptionally regulates *TP53INP1* and *TP53* is almost universally aberrant in

high-grade serous ovarian cancer. Importantly, some *TP53* mutations contribute to tumor progression through the acquisition of "gain-of-function" properties, which may explain the effects of miR569 (Freed-Pastor and Prives, 2012; Oren and Rotter, 2010). Furthermore, we show that p73 or NF-κB can transcriptionally regulate the expression of *TP53INP1* independent of p53. Compatible with this contention, *TP53INP1* levels were associated with outcomes in patients with high-grade serous ovarian cancers where *TP53* is almost universally mutant as well as in the subset of breast cancers with *TP53* mutations. Indeed, across multiple data sets, *TP53INP1* mRNA and proteins levels were associated with improved patient outcomes consistent with the ability of TP53INP1 to regulate apoptosis as well as the ability of miR569 to alter proliferation, anchorage independence, and multilamellar cellule formation.

It is unclear why manipulation of p53 altered proliferation and TP53INP1 levels in SV40 T-Ag transformed IOSE cells. However, a portion of p53 may not be completely inactivated by T-Ag and could potentially activate *TP53INP1* transcription directly (Deppert and Steinmayer, 1989; Sheppard et al., 1999). Alternatively, p53 complexed with T-Ag may form a functional complex with p63 or p73 thus regulating *TP53INP1* transcription (Urist and Prives, 2002).

The discovery that microRNAs are potent regulators of RNA stability and translation dramatically changed our understanding of the mechanisms controlling protein levels, and further provided a potential therapeutic approach to a number of targets that have previously been designated "undruggable." However, the translation of miR therapy to the clinic is in its infancy. Based on the effects of anti-miR569 in vitro and in vivo on cell survival in the presence and absence of cisplatin, the most commonly used drug in ovarian cancer, an approach to decrease miR569 activity or increase *TP53INP1* levels warrants exploration in ovarian and breast cancers. An ability to translate the in vivo anti-miR approaches used in the animal models herein to the patient would thus be highly attractive. Indeed, such studies are currently underway at the MD Anderson Cancer Center.

EXPERIMENTAL PROCEDURES

Patient Samples

After informed consent, normal ovarian epithelial tissues and serous epithelial ovarian cancer tissues were collected according to an Institutional Review Board approved protocol at the MD Anderson Cancer Center. Normal ovarian tissues were from the tumor-free ovary of patients with unilateral ovarian cancer or patients with other gynecological cancers not involving the ovary. After informed consent, normal fallopian tube tissue samples were collected according to an Institutional Review Board-approved protocol at the Harvard Cancer Center.

RNA Isolation and miR Detection

Total RNA from cultured cells, with efficient recovery of small RNAs, was isolated using the mirVana miR Isolation Kit (Ambion). Detection of mature miR was performed using cDNA generated with QIAGEN miScript kit and subsequent qRT-PCR analysis with SYBR

Green I (QIAGEN) according to manufacturers' instructions. Primers specific to mature microRNA sequences were from QIAGEN. The U6 small nuclear RNA (RNU6B) was used as internal normalization control.

MicroRNA Gene Overexpression

Human miR569 cloned into pEZX-MR06 lentiviral vector was from GeneCopoeia. Production of amphotropic viruses and infection of target cells were described previously (Stewart et al., 2003).

Oligonucleotide Transfection

The miRIDIAN microRNA mimics, double-stranded oligonucleotides designed to overexpress miRs, siRNAs targeting TP53INP1 and P53AIP1 (Dharmacon) and antimiR (Ambion) were transfected using Oligofectamine (Invitrogen).

AGO-PAR-CLIP Data Analysis

AGO-PAR-CLIP data analysis was performed as described previously (Hamilton et al., 2013). Detailed experimental procedures are provided in the Supplemental Experimental Procedures.

Cell Viability Assay

Cell viability (survival) was determined by a 2 hr incubation with 3-(4,5-dimethylthiazol-2-yl)-2,5-diphenyltetrazolium bromide (MTT), followed by lysis in acidic isopropanol (0.35% HCl in isopropanol) and measurement of absorbance at 570 nm. Cell viability was calculated as increase in MTT signal compared to MTT signal on Day 0 prior to treatment.

Morphogenesis Assay

Morphogenesis assays and anchorage-independent growth assays were performed as described previously (Pradeep et al., 2012a; Pradeep et al., 2012b). For 3D culture assays, trypsinized cells were resuspended in Dulbecco's modified Eagle's medium/F12 medium supplemented with 2% horse serum. Eight-chambered plates (BD Biosciences) were coated with 35 μl growth factor reduced Matrigel (BD Bioscience) per well. Cells were mixed with medium containing 4% Matrigel and plated at a final volume of 400 μl in each chamber.

Reverse-Phase Protein Arrays

Reverse-phase protein array analysis was performed as described previously (Hennessy et al., 2010) and detailed at http://www.mdanderson.org/education-and-research/resources-for-professionals/scientific-resources/core-facilities-and-services/functional-proteomics-rppa-core/index.html.

Indirect Immunofluorescence

Immunofluorescence analysis of acini was performed as described previously (Pradeep et al., 2012a). Acini were fixed in methanol-acetone and blocked in 10% goat serum. Secondary blocking was performed in buffer containing goat anti-mouse $F(ab')_2$ fragments

(20 μg/ml). Primary antibodies were incubated for 15–18 hr at 4°C and secondary antibodies for 1 hr before confocal microscopy.

Luciferase Reporter Assays

Cells were transfected with reporter plasmids or control vector using Lipofectamine 2000 (Invitrogen). Twenty-four hours after transfection, cells were washed twice with PBS and then lysed and luciferase activity measured using luciferase assay substrate (Promega) according to the manufacturer's protocol using an Opticom II luminometer (MGM Instruments).

Cytochrome C Analysis

Cytochrome-C release kit was from Kamiya Biomedical. Cells were collected after treatment and suspended in cytosol extraction buffer mix containing protease inhibitors and incubated for 10 min on ice. Homogenates were collected and centrifuged at 700 × *g* for 10 min at 4°C. Supernatants were collected into a fresh 1.5 ml tube, and centrifuged at 10,000 × *g* for 30 min at 4°C. Supernatants were collected and released cytochrome C was assessed using an ELISA kit from R&D Systems.

Analysis of Public Gene Expression Data Sets

TCGA ovarian cancer SNP, mRNA data, TCGA breast cancer reverse-phase protein arrays, and clinical data were downloaded from the TCGA Data portal (http://tcga-data.nci.nih.gov/tcga/findArchives.htm). "Amplification" was defined as gain of more than three copies and "copy number gain" as gain of at least 0.5 copies, respectively. CNTools package from Bioconductor (http://www.bioconductor.org/) was used to process SNP data. Cox proportional hazard regression model was used for univariate survival analysis. Overall survival or recurrence-free survival was used as an endpoint. The cutoffs of high expression and low expression were optimized to achieve the lowest p value. Statistical analysis was performed using R Software.

Animal Studies

Female athymic nude mice were from the National Cancer Institute, Frederick Cancer Research and Development Center. Animals were cared for according to guidelines set forth by the American Association for Accreditation of Laboratory Animal Care and the US Public Health Service policy on Human Care and Use of Laboratory Animals. All mouse studies were approved and supervised by the MD Anderson Cancer Center Institutional Animal Care and Use Committee.

Additional experimental protocols are described in the Supplemental Experimental Procedures.

Supplementary Material

Refer to Web version on PubMed Central for supplementary material.

Acknowledgments

G.B.M. is supported by NCI (2P50CA083639-11, 5P50CA058183-17, and 5R01CA123219-01), Stand up to Cancer/American Association of Cancer Research (SU2C-AACR-DT0209), and Komen Promise Grant (KG081694). P.C.R. is supported by Ann Schreiber Program for Excellence grant from Ovarian Cancer Research Fund and Scientific scholar award from Marsha Rivkin Center for Ovarian Cancer Research. J.W.G. is supported by NCI (P50CA58207 and U54CA112970). A.K.S. is supported by NCI (P50CA083639, P50CA098258, and U54CA151668). We thank Lydia W.T. Cheung for helpful insights. We acknowledge technical help from Nitin Puri and Varun Bagai, Ambion, Life Technologies, Austin, Texas for the RNAi studies. We thank Ronny Drapkin, Marian Novak, and Alison Karst for providing RNA extracted from normal fallopian tube samples. G.B.M. received sponsored research support from AstraZeneca, GlaxoSmithKline, Celgene, Exelixis, Roche, and Wyeth/Pfizer and has served as consultant to AstraZeneca, Celgene, Enzon, Hanall Bio, Novartis, Nuevolution, Symphogen, and Wyeth/Pfizer.

References

Bagnoli M, De Cecco L, Granata A, Nicoletti R, Marchesi E, Alberti P, Valeri B, Libra M, Barbareschi M, Raspagliesi F, et al. Identification of a chrXq27.3 microRNA cluster associated with early relapse in advanced stage ovarian cancer patients. Oncotarget. 2011; 2:1265–1278. [PubMed: 22246208]

Bentink S, Haibe-Kains B, Risch T, Fan JB, Hirsch MS, Holton K, Rubio R, April C, Chen J, Wickham-Garcia E, et al. Angiogenic mRNA and microRNA gene expression signature predicts a novel subtype of serous ovarian cancer. PLoS ONE. 2012; 7:e30269. [PubMed: 22348002]

Cancer Genome Atlas Research Network. Comprehensive molecular portraits of human breast tumours. Nature. 2012; 490:61–70. [PubMed: 23000897]

Cancer Genome Atlas Research Network. Integrated genomic analyses of ovarian carcinoma. Nature. 2011; 474:609–615. [PubMed: 21720365]

Chi SW, Zang JB, Mele A, Darnell RB. Argonaute HITS-CLIP decodes microRNA-mRNA interaction maps. Nature. 2009; 460:479–486. [PubMed: 19536157]

Ciriello G, Miller ML, Aksoy BA, Senbabaoglu Y, Schultz N, Sander C. Emerging landscape of oncogenic signatures across human cancers. Nat Genet. 2013; 45:1127–1133. [PubMed: 24071851]

Deppert W, Steinmayer T. Metabolic stabilization of p53 in SV40-transformed cells correlates with expression of the transformed phenotype but is independent from complex formation with SV40 large T antigen. Curr Top Microbiol Immunol. 1989; 144:77–83. [PubMed: 2551594]

Eder AM, Sui X, Rosen DG, Nolden LK, Cheng KW, Lahad JP, Kango-Singh M, Lu KH, Warneke CL, Atkinson EN, et al. Atypical PKCiota contributes to poor prognosis through loss of apical-basal polarity and cyclin E overexpression in ovarian cancer. Proc Natl Acad Sci USA. 2005; 102:12519–12524. [PubMed: 16116079]

Enerly E, Steinfeld I, Kleivi K, Leivonen SK, Aure MR, Russnes HG, Rønneberg JA, Johnsen H, Navon R, Rødland E, et al. miRNA-mRNA integrated analysis reveals roles for miRNAs in primary breast tumors. PLoS ONE. 2011; 6:e16915. [PubMed: 21364938]

Esquela-Kerscher A, Slack FJ. Oncomirs - microRNAs with a role in cancer. Nat Rev Cancer. 2006; 6:259–269. [PubMed: 16557279]

Flores ER, Tsai KY, Crowley D, Sengupta S, Yang A, McKeon F, Jacks T. p63 and p73 are required for p53-dependent apoptosis in response to DNA damage. Nature. 2002; 416:560–564. [PubMed: 11932750]

Freed-Pastor WA, Prives C. Mutant p53: one name, many proteins. Genes Dev. 2012; 26:1268–1286. [PubMed: 22713868]

Gasco M, Shami S, Crook T. The p53 pathway in breast cancer. Breast Cancer Res. 2002; 4:70–76. [PubMed: 11879567]

Gironella M, Seux M, Xie MJ, Cano C, Tomasini R, Gommeaux J, Garcia S, Nowak J, Yeung ML, Jeang KT, et al. Tumor protein 53-induced nuclear protein 1 expression is repressed by miR-155, and its restoration inhibits pancreatic tumor development. Proc Natl Acad Sci USA. 2007; 104:16170–16175. [PubMed: 17911264]

Gommeaux J, Cano C, Garcia S, Gironella M, Pietri S, Culcasi M, Pébusque MJ, Malissen B, Dusetti N, Iovanna J, Carrier A. Colitis and colitis-associated cancer are exacerbated in mice deficient for

tumor protein 53-induced nuclear protein 1. Mol Cell Biol. 2007; 27:2215–2228. [PubMed: 17242209]

Greenblatt MS, Bennett WP, Hollstein M, Harris CC. Mutations in the p53 tumor suppressor gene: clues to cancer etiology and molecular pathogenesis. Cancer Res. 1994; 54:4855–4878. [PubMed: 8069852]

Haakensen VD, Biong M, Lingjærde OC, Holmen MM, Frantzen JO, Chen Y, Navjord D, Romundstad L, Lüders T, Bukholm IK, et al. Expression levels of uridine 5′-diphospho-glucuronosyltransferase genes in breast tissue from healthy women are associated with mammographic density. Breast Cancer Res. 2010; 12:R65. [PubMed: 20799965]

Hafner M, Landthaler M, Burger L, Khorshid M, Hausser J, Berninger P, Rothballer A, Ascano M Jr, Jungkamp AC, Munschauer M, et al. Transcriptome-wide identification of RNA-binding protein and microRNA target sites by PAR-CLIP. Cell. 2010; 141:129–141. [PubMed: 20371350]

Hamilton MP, Rajapakshe K, Hartig SM, Reva B, McLellan MD, Kandoth C, Ding L, Zack TI, Gunaratne PH, Wheeler DA, et al. Identification of a pan-cancer oncogenic microRNA superfamily anchored by a central core seed motif. Nat Commun. 2013; 4:2730. [PubMed: 24220575]

Hennessy BT, Lu Y, Gonzalez-Angulo AM, Carey MS, Myhre S, Ju Z, Davies MA, Liu W, Coombes K, Meric-Bernstam F, et al. A technical assessment of the utility of reverse phase protein arrays for the study of the functional proteome in non-microdissected human breast cancers. Clin Proteomics. 2010; 6:129–151. [PubMed: 21691416]

Komurov K, Dursun S, Erdin S, Ram PT. NetWalker: a contextual network analysis tool for functional genomics. BMC Genomics. 2012; 13:282. [PubMed: 22732065]

Landen CN Jr, Chavez-Reyes A, Bucana C, Schmandt R, Deavers MT, Lopez-Berestein G, Sood AK. Therapeutic EphA2 gene targeting in vivo using neutral liposomal small interfering RNA delivery. Cancer Res. 2005; 65:6910–6918. [PubMed: 16061675]

Langerød A, Zhao H, Borgan Ø, Nesland JM, Bukholm IR, Ikdahl T, Kåresen R, Børresen-Dale AL, Jeffrey SS. TP53 mutation status and gene expression profiles are powerful prognostic markers of breast cancer. Breast Cancer Res. 2007; 9:R30. [PubMed: 17504517]

Lewis BP, Burge CB, Bartel DP. Conserved seed pairing, often flanked by adenosines, indicates that thousands of human genes are microRNA targets. Cell. 2005; 120:15–20. [PubMed: 15652477]

Liang J, Nagahashi M, Kim EY, Harikumar KB, Yamada A, Huang WC, Hait NC, Allegood JC, Price MM, Avni D, et al. Sphingosine-1-phosphate links persistent STAT3 activation, chronic intestinal inflammation, and development of colitis-associated cancer. Cancer Cell. 2013; 23:107–120. [PubMed: 23273921]

Muggerud AA, Hallett M, Johnsen H, Kleivi K, Zhou W, Tahmasebpoor S, Amini RM, Botling J, Børresen-Dale AL, Sørlie T, Wärnberg F. Molecular diversity in ductal carcinoma in situ (DCIS) and early invasive breast cancer. Mol Oncol. 2010; 4:357–368. [PubMed: 20663721]

Muranen T, Selfors LM, Worster DT, Iwanicki MP, Song L, Morales FC, Gao S, Mills GB, Brugge JS. Inhibition of PI3K/mTOR leads to adaptive resistance in matrix-attached cancer cells. Cancer Cell. 2012; 21:227–239. [PubMed: 22340595]

Nanjundan M, Cheng KW, Zhang F, Lahad J, Kuo WL, Schmandt R, Smith-McCune K, Fishman D, Gray JW, Mills GB. Overexpression of SnoN/SkiL, amplified at the 3q26.2 locus, in ovarian cancers: a role in ovarian pathogenesis. Mol Oncol. 2008; 2:164–181. [PubMed: 19383336]

Naume B, Zhao X, Synnestvedt M, Borgen E, Russnes HG, Lingjaerde OC, Strømberg M, Wiedswang G, Kvalheim G, Kåresen R, et al. Presence of bone marrow micrometastasis is associated with different recurrence risk within molecular subtypes of breast cancer. Mol Oncol. 2007; 1:160–171. [PubMed: 19383292]

Okamura S, Arakawa H, Tanaka T, Nakanishi H, Ng CC, Taya Y, Monden M, Nakamura Y. p53DINP1, a p53-inducible gene, regulates p53-dependent apoptosis. Mol Cell. 2001; 8:85–94. [PubMed: 11511362]

Oren M, Rotter V. Mutant p53 gain-of-function in cancer. Cold Spring Harb Perspect Biol. 2010; 2:a001107. [PubMed: 20182618]

Pawitan Y, Bjöhle J, Amler L, Borg AL, Egyhazi S, Hall P, Han X, Holmberg L, Huang F, Klaar S, et al. Gene expression profiling spares early breast cancer patients from adjuvant therapy: derived

and validated in two population-based cohorts. Breast Cancer Res. 2005; 7:R953–R964. [PubMed: 16280042]

Pradeep CR, Köstler WJ, Lauriola M, Granit RZ, Zhang F, Jacob-Hirsch J, Rechavi G, Nair HB, Hennessy BT, Gonzalez-Angulo AM, et al. Modeling ductal carcinoma in situ: a HER2-Notch3 collaboration enables luminal filling. Oncogene. 2012a; 31:907–917. [PubMed: 21743488]

Pradeep CR, Zeisel A, Köstler WJ, Lauriola M, Jacob-Hirsch J, Haibe-Kains B, Amariglio N, Ben-Chetrit N, Emde A, Solomonov I, et al. Modeling invasive breast cancer: growth factors propel progression of HER2-positive premalignant lesions. Oncogene. 2012b; 31:3569–3583. [PubMed: 22139081]

Schafer ZT, Grassian AR, Song L, Jiang Z, Gerhart-Hines Z, Irie HY, Gao S, Puigserver P, Brugge JS. Antioxidant and oncogene rescue of metabolic defects caused by loss of matrix attachment. Nature. 2009; 461:109–113. [PubMed: 19693011]

Sheppard HM, Corneillie SI, Espiritu C, Gatti A, Liu X. New insights into the mechanism of inhibition of p53 by simian virus 40 large T antigen. Mol Cell Biol. 1999; 19:2746–2753. [PubMed: 10082540]

Stewart SA, Dykxhoorn DM, Palliser D, Mizuno H, Yu EY, An DS, Sabatini DM, Chen IS, Hahn WC, Sharp PA, et al. Lentivirus-delivered stable gene silencing by RNAi in primary cells. RNA. 2003; 9:493–501. [PubMed: 12649500]

Tomasini R, Samir AA, Vaccaro MI, Pebusque MJ, Dagorn JC, Iovanna JL, Dusetti NJ. Molecular and functional characterization of the stress-induced protein (SIP) gene and its two transcripts generated by alternative splicing. SIP induced by stress and promotes cell death. J Biol Chem. 2001; 276:44185–44192. [PubMed: 11557757]

Tomasini R, Samir AA, Carrier A, Isnardon D, Cecchinelli B, Soddu S, Malissen B, Dagorn JC, Iovanna JL, Dusetti NJ. TP53INP1s and homeodomain-interacting protein kinase-2 (HIPK2) are partners in regulating p53 activity. J Biol Chem. 2003; 278:37722–37729. [PubMed: 12851404]

Tomasini R, Seux M, Nowak J, Bontemps C, Carrier A, Dagorn JC, Pébusque MJ, Iovanna JL, Dusetti NJ. TP53INP1 is a novel p73 target gene that induces cell cycle arrest and cell death by modulating p73 transcriptional activity. Oncogene. 2005; 24:8093–8104. [PubMed: 16044147]

Tothill RW, Tinker AV, George J, Brown R, Fox SB, Lade S, Johnson DS, Trivett MK, Etemadmoghadam D, Locandro B, et al. Australian Ovarian Cancer Study Group. Novel molecular subtypes of serous and endometrioid ovarian cancer linked to clinical outcome. Clin Cancer Res. 2008; 14:5198–5208. [PubMed: 18698038]

Urist M, Prives C. p53 leans on its siblings. Cancer Cell. 2002; 1:311–313. [PubMed: 12086844]

Weber-Mangal S, Sinn HP, Popp S, Klaes R, Emig R, Bentz M, Mansmann U, Bastert G, Bartram CR, Jauch A. Breast cancer in young women (< or = 35 years): Genomic aberrations detected by comparative genomic hybridization. Int J Cancer. 2003; 107:583–592. [PubMed: 14520696]

Yang JH, Li JH, Jiang S, Zhou H, Qu LH. ChIPBase: a database for decoding the transcriptional regulation of long non-coding RNA and microRNA genes from ChIP-Seq data. Nucleic Acids Res. 2013; 41:D177–D187. [PubMed: 23161675]

Significance

DNA copy number aberrations (CNAs) drive tumorigenesis across cancer lineages. Although some CNAs are narrow, targeting a discrete set of genes, others such as the 3q26.2 amplicon, which is present in ~35% of high-grade serous ovarian cancers and ~15% of breast cancers, primarily in aggressive basal-like breast tumors, as well as several other tumor lineages, are broad and likely contain multiple driver aberrations. We demonstrate that the 3q26.2 amplicon increases miR569 levels with subsequent decreases in *TP53INP1*, contributing to proliferation and survival of epithelial cancer cells in vitro and in vivo. Thus, miR569 and its target *TP53INP1* are promising candidate biomarkers and therapeutic targets.

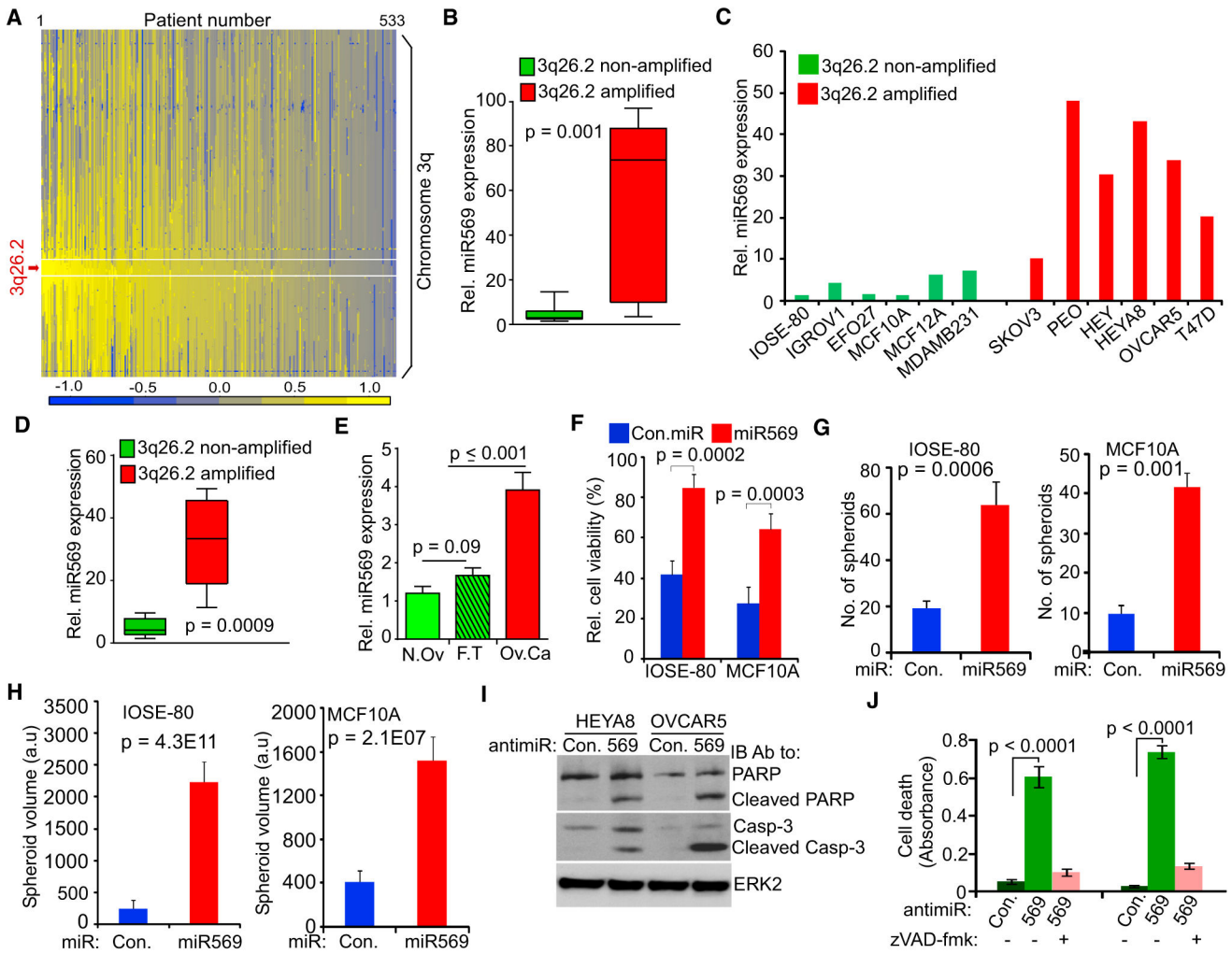

Figure 1. Amplification of 3q26.2 Correlates with miR569 Expression and Increases Proliferation of Ovarian Cancer Cells

(A) Heatmap of copy number alterations of chromosome 3q in 533 ovarian cancer samples. Red arrow indicates the 3q26.2 region.

(B) miR569 expression in ovarian cancer samples (n = 33) assessed by quantitative real-time PCR (qRT-PCR). Box plot represents lower quartile; median and upper quartile and whiskers represent the 95% confidence interval of the mean. Significance was calculated with Student's t test.

(C) Expression of miR569 in cell lines assessed by qRT-PCR.

(D) miR569 expression in cell lines presented in Figure 1C. Box plot represents lower quartile; median and upper quartile and whiskers represent the 95% confidence interval of the mean. Significance was calculated with Student's t test.

(E) miR569 expression in normal ovarian (N. Ov), fallopian tube (F. T) or ovarian cancer (Ov. Ca) epithelium was analyzed by qRT-PCR and normalized to U6 RNA (n = 8 per group). Bars represent mean ± SEM. Significance was calculated with Student's t test.

(F) Cell viability of IOSE-80 and MCF10A transfected with control oligos or miR569 was assessed on day 4 using 3-(4,5-dimethylthiazol-z-yl)-2,5-diphenyl tetrazolium bromide

(MTT). Bars represent SD of quadruplicates. Significance was calculated with Student's t test.

(G and H) IOSE-80 cells were grown in suspension on low attachment plates for 2 days in low density conditions. Colonies were photographed 4 days after transfection with control miR or miR569. MCF10A grown on Matrigel for 2 days were infected with lentivirus of human miR569 or control miR and allowed to grow on Matrigel for another 10 days. Spheroids were fixed and photographed. Number (G) and volume (H) of spheroids were calculated using Nikon Elements digital imaging software. Bars represent SD of images from three different fields.

(I) HEYA8 or OVCAR5 were lysed 48 hr after transfection with control antimiR or anti-miR569 and immunoblotted with indicated antibodies.

(J) Cell death was assessed using Roche's Cell Death Detection ELISA kit 72 hr after antimiR transfection in presence or absence of pan-caspase inhibitor. Bars represent SD of quadruplicates. Significance was calculated with Student's t test.

See also Figure S1 and Table S1.

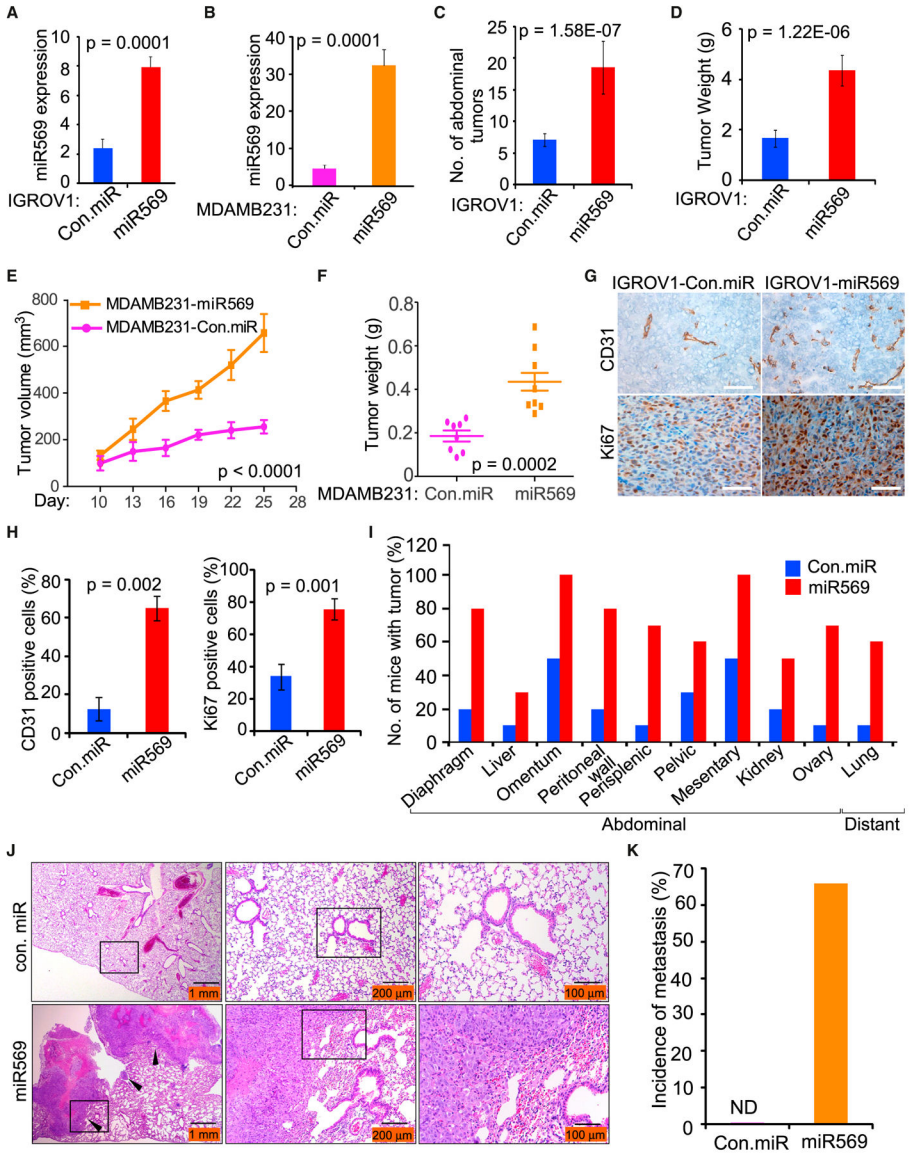

Figure 2. miR569 Promotes Tumor Growth and Metastasis In Vivo

(A) IGROV1 cells stably expressing miR569 or control miR by lentiviral transduction were harvested for qRT-PCR to analyze miR569 expression. Bars represent SD of triplicates. Significance was calculated with Student's t test.

(B) MDAMB231 stably expressing miR569 or control miR by lentiviral transduction were harvested for qRT-PCR to analyze miR569 expression. Bars represent SD of triplicates.

(C and D) IGROV1 cells stably expressing miR569 or control miR were injected into the peritoneal cavity of female nude mice (n = 10 per group). Tumors were isolated on day 35 and number of abdominal tumors (C) and tumor weight (D) assessed. Bars represent SEM and significance was calculated with unpaired Student's t test.

(E and F) MDAMB231 stably expressing miR569 or control miR were injected into mammary fat pads of female nude mice (n = 8 per group); tumor volume was calculated at indicated time points (E, n = 8 per group). On day 25, tumors were isolated and tumor

weight determined (F). Bars represent SEM. Significance was calculated with Student's t test.

(G and H) Representative immunohistochemical staining (G) and statistical analysis (H; n = 3) of CD31 and Ki67 of tumors from mice in (C) and (D). Scale bars represent 50 μm. Bars represent SD of triplicates. Significance was calculated with Student's t test.

(I) Sites of tumor growth from mice in (C) and (D).

(J) Haematoxylin and eosin staining of six lung tissues isolated from (E); black arrows indicate metastases to the lung. Black squares are magnified and displayed on the right of indicated groups.

(K) Metastasis incidence of mice in (E). Significance was by Fisher's exact test. ND, not detected.

See also Figure S2.

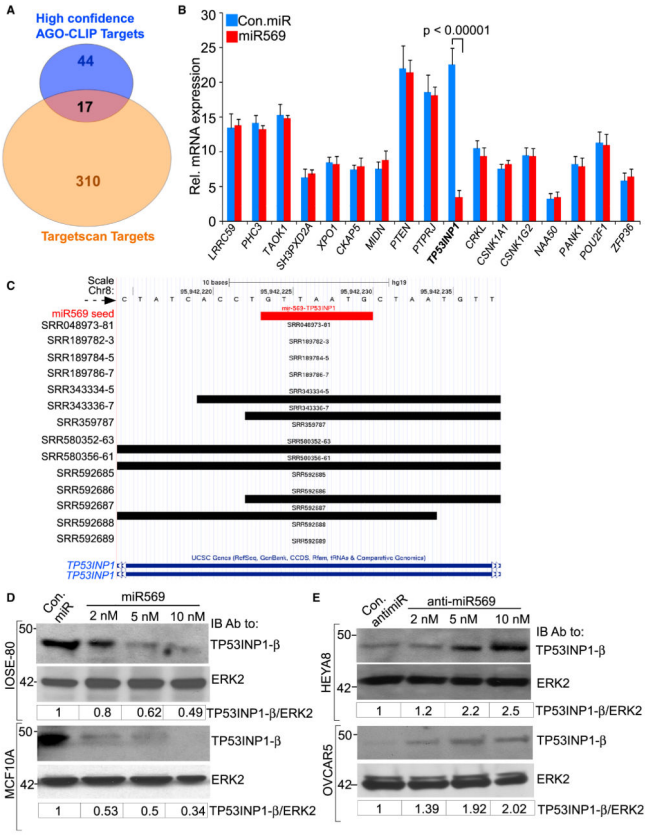

Figure 3. Integrative Genomic Approach Identifies *TP53INP1* as a Target of miR569

(A) Venn diagrams of putative miR569 targets predicted by TargetScan and high confidence targets identified with AGO-CLIP.

(B) IOSE-80 cells were transfected with control miR or miR569 and total RNA isolated after 24 hr. Seventeen genes common to Targetscan and AGO-CLIP from (A) were assessed by qRT-PCR and normalized to *ACTB* mRNA. Bars represent SD of triplicates. Significance was calculated with Student's t test comparing miR569 treated group with control.

(C) Black lines indicate active miR569 target sites on the *TP53INP1* 3′UTR in 6 out of 14 AGO-CLIP publicly available data sets.

(D) IOSE-80 and MCF10A transfected with control miR or miR569 for 48 hr were lysed for immunoblotting with indicated antibodies.

(E) HEYA8 and OVCAR5 transfected with control miR or miR569 for 48 hr were lysed for immunoblotting.

See also Tables S2, S3, and S4.

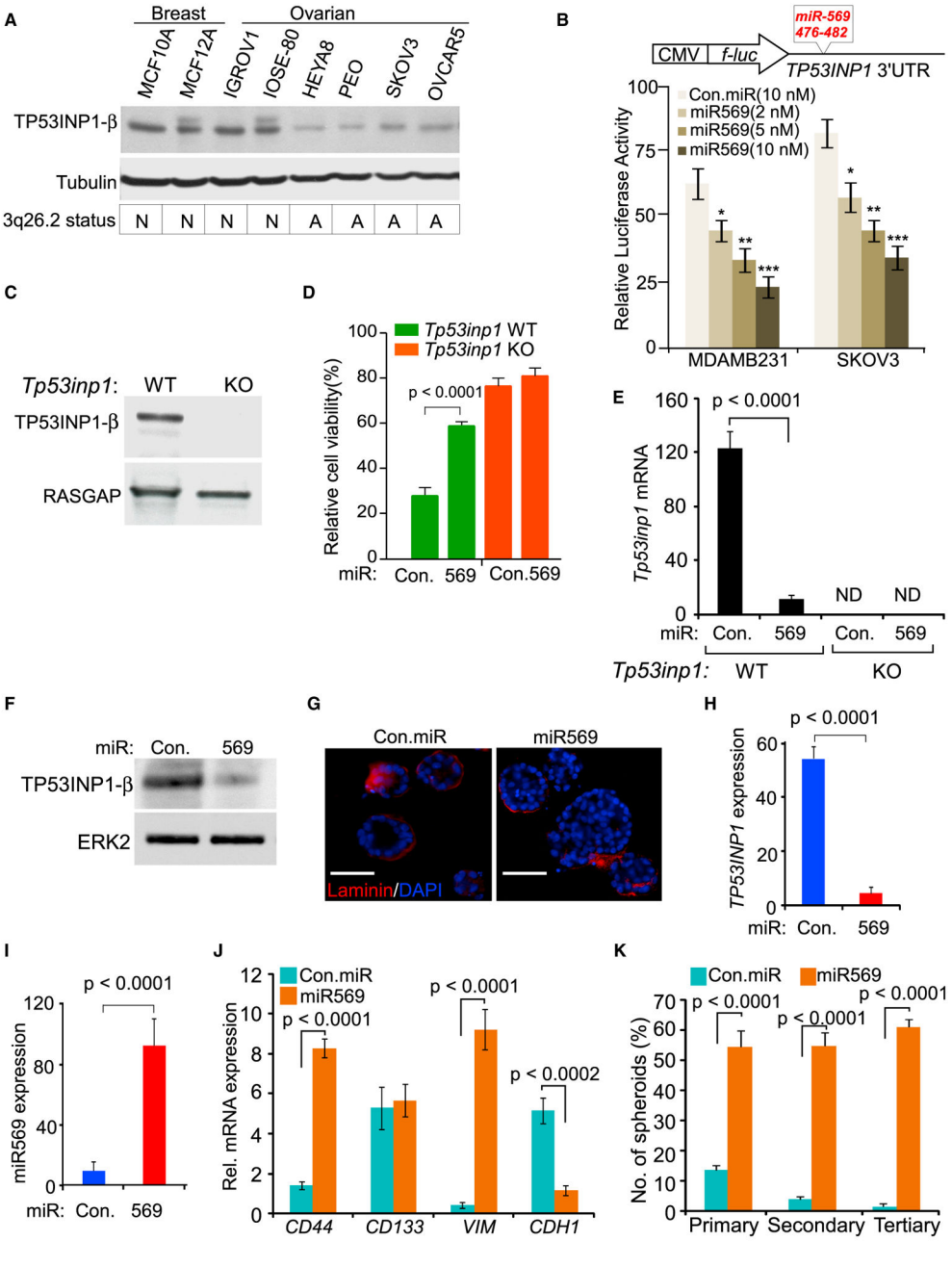

Figure 4. miR569 Regulates *TP53INP1* Expression by Binding the 3′UTR and Controls Proliferation of Breast and Ovarian Cells

(A) Immunoblot of TP53INP1 level and 3q26.2 copy number status of indicated cell lines. N and A represent 3q26.2 nonamplified or amplified, respectively (see Figure 1C).

(B) *TP53INP1* 3′UTR luciferase reporter construct (top) was cotransfected with control miR or miR569 into MDAMB231 or SKOV3 and luciferase activity was assessed (bottom). Bars represent SD of quadruplicates. Significance was calculated with Student's t test. *$p \leq 0.01$, **$p < 0.005$, and ***$p < 0.0005$.

(C) Wild-type (WT) or *Tp53inp1* knockout (KO) MEFs were lysed and immunoblotted with TP53INP1 and RASGAP (loading control) antibodies.
(D) WT *or Tp53inp1* KO MEFs were transfected with control miR or miR569. Cell viability was assessed on day 4. Bars represent SD of triplicates. Significance was by Student's t test comparing miR569 treated with control.
(E) mRNA was extracted from WT or *Tp53inp1* KO MEFs 24 hr after transfection with control miR or miR569. *Tp53inp1* mRNA level was analyzed by qRT-PCR and normalized to that of *Actb* mRNA. ND, not detected.
(F) Immunoblots of WT MEFs transfected with control miR or miR569.
(G) MCF10A grown as spheroids in 5% Matrigel for 12 days were transfected with control miR or miR569 and cultured for another 72 hr. Spheroids were fixed and stained using DAPI. Images were captured using confocal microscopy. Scale bars represent 100 μm.
(H and I) *TP53INP1* (H) or miR569 (I) levels of MCF10A spheroids transfected with control miR or miR569 were analyzed by qRT-PCR and normalized to *ACTB* mRNA or U6 RNA control, respectively. Bars represent SD of triplicates. Significance was calculated with Student's t test.
(J) MCF10A grown in 5% Matrigel for 12 days were transfected with control miR or miR569 and cultured for another 72 hr. Total RNA was extracted from spheroids and expression of target genes assessed by qRT-PCR and normalized to *ACTB* mRNA. Bars represent SD of triplicate determinations. Significance was calculated with Student's t test.
(K) Spheroids grown as described in (J) were trypsinized and replated twice after 12-day intervals. Number of spheroids (%) formed in each cycle was quantified. Bars represent SD of triplicate determinations. Significance was calculated with Student's t test.
See Figure S3.

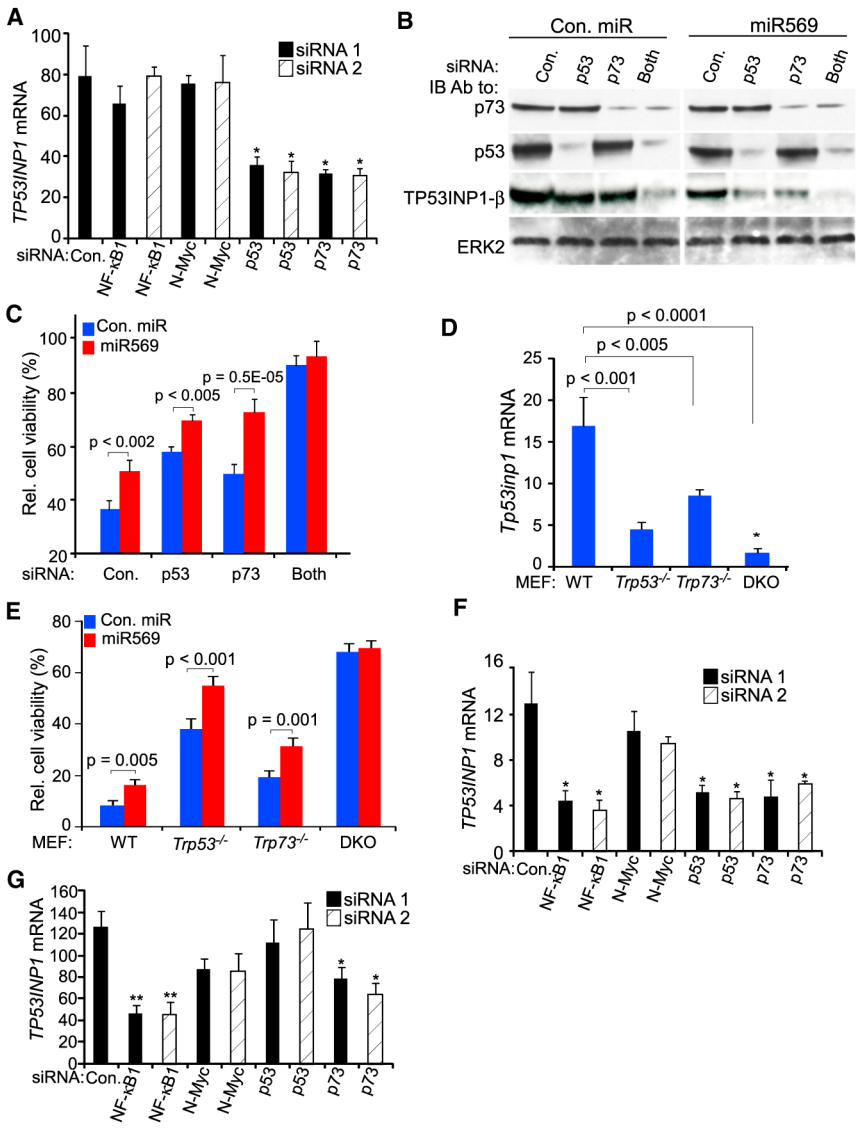

Figure 5. miR569 Exerts Growth Effects by Altering Expression of *TP53INP1* Induced by p53 or p73

(A) IOSE-80 cells were lysed 48 hr after transfection with control or indicated siRNA, and *TP53INP1* mRNA expression was quantified by qRT-PCR and normalized to *ACTB* mRNA. Bars represent SD of triplicates. Significance was calculated with Student's t test.

(B) IOSE-80 cells were transfected with control miR or miR569 24 hr after transfection with siRNA specific to p53 or p73 or both. Cells were lysed 48 hr after miR569 transfection and immunoblotted with the indicated antibodies.

(C) IOSE-80 cells were transfected as indicated in (B) and viable cell number monitored 72 hr after miR569 transfection using MTT. Bars represent SD of quadruplicates. Significance was calculated with Student's t test.

(D) Total RNA was extracted from MEFs from knock-out mice: *Trp53*$^{-/-}$, *Trp73*$^{-/-}$, or *Trp53*$^{-/-}$*: Trp73*$^{-/-}$ (DKO). *Tp53inp1* expression was analyzed by qRT-PCR and

normalized to *Actb* mRNA. Bars represent SD of triplicates. Significance was calculated with Student's t test. *p ≤ 0.005 compared to *Trp53*$^{-/-}$ or *Trp73*$^{-/-}$ MEFs.

(E) Cell viability of MEFs described in Figure 4D was assessed 72 hr after transfection with miR569 or control miR. Bars represent SD of quadruplicates. Significance was calculated with Student's t test.

(F and G) HEYA8 (F) or OVCAR5 (G) were lysed 48 hr after transfection with control or indicated siRNA. *TP53INP1* mRNA quantified by qRT-PCR. Bars represent SD of triplicates. Significance was tested calculated with Student's t test. *p < 0.01, **p < 0.005 compared to control siRNA.

See Figure S4.

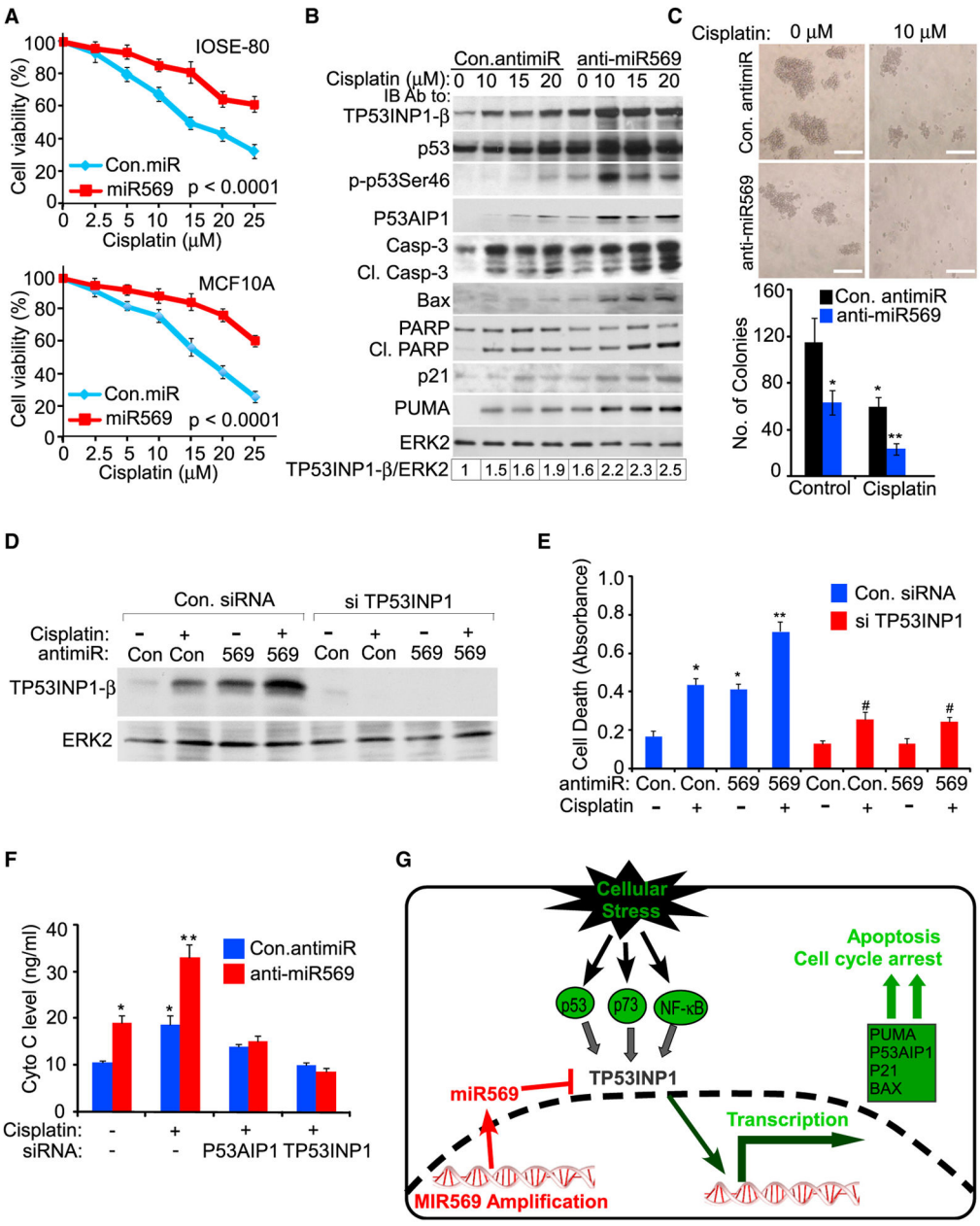

Figure 6. Anti-miR569 Sensitizes Ovarian Cancer Cells to Cisplatin Treatment

(A) IOSE-80 and MCF10A were transfected with control miR or miR569 24 hr prior to cisplatin treatment at indicated concentrations. Cell viability was monitored 72 hr after transfection using MTT. Bars represent SD of triplicates. Significance was by two-way ANOVA.

(B) HEYA8 (WT *TP53*) transfected with control antimiR or anti-miR569 for 48 hr were treated with cisplatin for another 8 hr before immunoblotting using indicated antibodies.

(C) HEYA8 cells grown on low attachment plates in low density for 7 days were transfected with control antimiR or anti-miR569 for another 48 hr prior to addition of cisplatin (top). Colonies were photographed 4 days after cisplatin addition (bottom). Scale bars represent

100 μm. Number of colonies formed was quantified. Bars represent SD of triplicates. Significance was calculated with Student's t test. *$p \leq 0.005$, **$p < 0.001$.

(D and E) HEYA8 cells were transfected with control or TP53INP1 specific siRNA 24 hr prior to antimiR transfection. Cells were treated with 10 μM cisplatin for 48 hr after antimiR transfection, lysed and immunoblotted using indicated antibodies (D), and cell death was assessed using a cell death ELISA 72 hr after antimiR treatment (E). Bars represent SD of quadruplicates. Significance was calculated with Student's t test. *$p < 0.001$, **$p < 0.0001$ compared to control oligo transfected group without cisplatin. $^{\#}p < 0.01$ compared to cisplatin or anti-miR569 group.

(F) HEYA8 were transfected with siRNAs specific to TP53INP1 or P53AIP1 24 hr prior to transfection with antimiR. Cells were treated with 10 μM cisplatin for 48 hr after antimiR transfection. Cytosolic fractions were prepared and cytochrome C quantitated by ELISA. Bars represent SD of triplicates. *$p < 0.01$, **$p < 0.005$ compared to control antimiR transfected group without cisplatin.

(G) Proposed model illustrates deregulation of cell cycle and proliferation by miR569. See Figure S5.

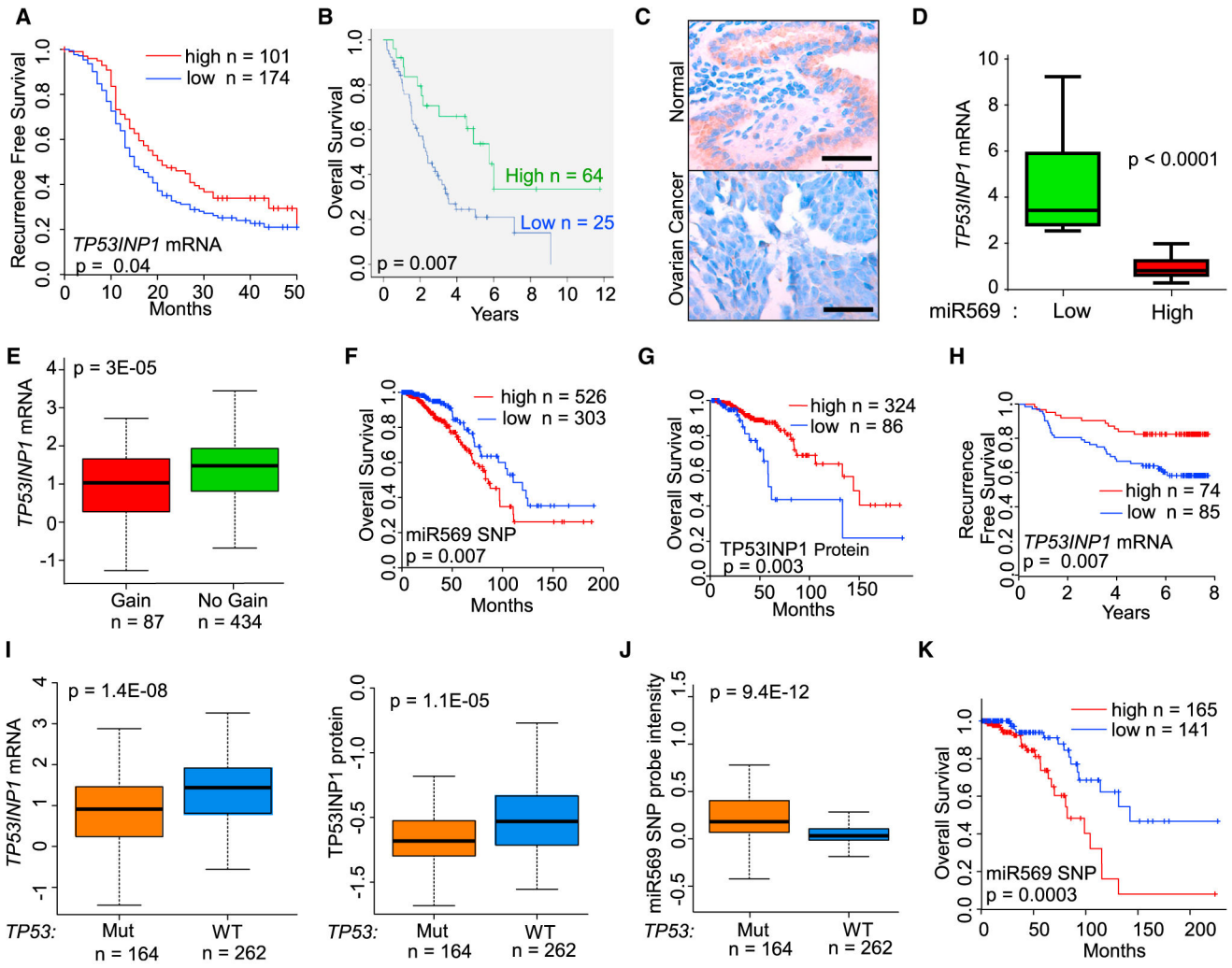

Figure 7. miR569 Copy Number Changes and *TP53INP1* Expression Are Associated with Ovarian and Breast Cancer Outcomes

(A) Kaplan-Meier plot of recurrence-free survival (RFS) of 275 patients with ovarian cancer (Tothill et al., 2008) stratified by high or low *TP53INP1* expression in tumor.

(B) Kaplan-Meier plot of overall survival of 89 patients with ovarian cancer stratified by high or low TP53INP1 protein levels in their tumors determined by immunohistochemistry (IHC). Log-rank test was used to compare differences between groups.

(C) IHC images of TP53INP1 expression in ovarian cancer tissue and normal tissue. Scale bars represent 50 μm.

(D) *TP53INP1* expression in 33 ovarian cancers assessed by qRT-PCR and normalized to *ACTB* mRNA. Box plot represents lower quartile; median and upper quartile and whiskers represent the 95% confidence interval of the mean. Significance was calculated with Student's t test.

(E) *TP53INP1* mRNA levels in 521 TCGA breast cancer samples based on miR569 copy number levels. Box plot represents lower, median, and upper quartiles. Whiskers represent the upper or lower quartile plus 1.5 times the interquartile range. Significance was calculated with two-tailed Student's t test.

(F) Kaplan-Meir analysis of overall survival based on miR569 copy number alterations from TCGA (n = 829). Significance was calculated with log-rank test.
(G) Kaplan-Meier plot of overall survival of 410 patients with breast cancer based on tumor TP53INP1 protein levels from TCGA RPPA data. Significance was calculated with log-rank test.
(H) Kaplan-Meier plot of recurrence-free survival of patients with breast cancer (n = 159) stratified by high or low *TP53INP1* mRNA expression in a published breast cancer data set (Pawitan et al., 2005). Significance was calculated with log-rank test.
(I) Expression of *TP53INP1* mRNA and protein levels in TCGA breast cancer data of *TP53* mutated (Mut) or wild-type (WT) samples. Significance was calculated with two-tailed t test.
(J) miR569 copy number alterations in TCGA breast cancer data of *TP53* Mut or WT samples. Significance was calculated with two-tailed t test. Box plot in (I) and (J) represents lower, median, and upper quartiles. Whiskers represent the upper or lower quartile plus 1.5 times the interquartile range.
(K) Kaplan-Meir plot of overall survival based on miR569 copy number alterations of 306 breast cancer tumors with WT *TP53* from TCGA breast cancer data. Note: size of TCGA sample sets vary due to availability of data and changes in analysis platforms.
See Figure S6.

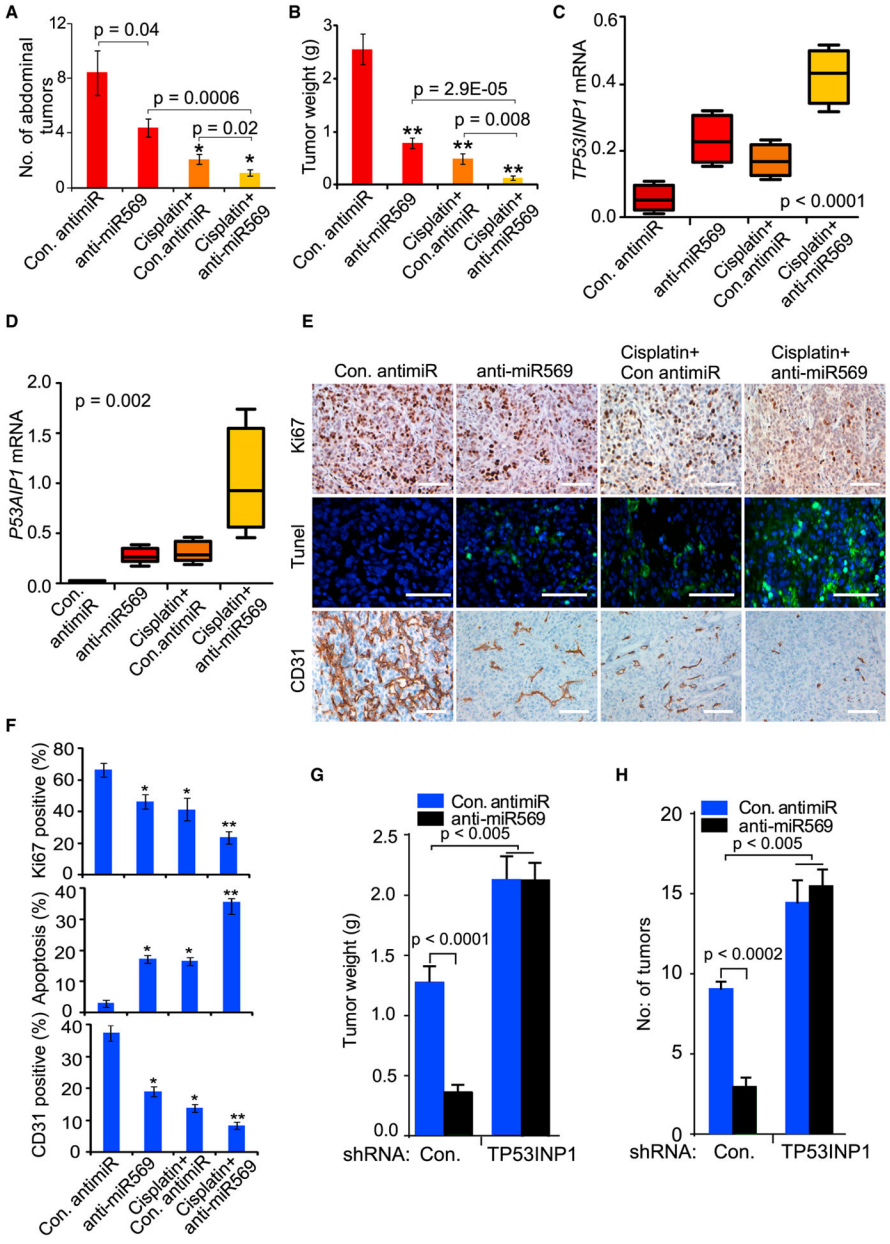

Figure 8. Liposomal Anti-miR569 Delivery Inhibits Tumor Growth and Abdominal Metastasis of HEYA8 Cells In Vivo

(A and B) HEYA8 cells (2.5×10^5 cells/animal) were injected intraperitoneally. Mice were treated with control antimiR, anti-miR569, cisplatin, or cisplatin combined with anti-miR569 (n = 10 per group). Numbers of abdominal tumors (A) and total tumor weight (B) were calculated. Bars represent SEM. Significance was calculated with Student's t test. *p < 0.001, **p < 0.0001 compared to control antimiR treated mice (n = 10 per group).

(C and D) RNA was extracted from four samples of each group in quadruplicate. Relative expression of *TP53INP1* (C) and *P53AIP1* (D) was analyzed by qRT-PCR and normalized to *ACTB* mRNA. Box plot represents lower quartile; median and upper quartiles and

whiskers represent the 95% confidence interval of the mean. Significance was calculated with one-way ANOVA.

(E) In vivo effects of anti-miR569 treatment on tumor cell proliferation and angiogenesis were determined by immunohistochemistry (IHC) of Ki67, CD31, and TUNEL for apoptosis. Scale bars represent 50 μm.

(F) Significance of IHC and TUNEL staining of tissues from (Figure 6F) using Student's t test. Bars represent SD of triplicates. *$p < 0.005$, **$p < 0.0001$ compared to control antimiR-treated mice. Combined treatments were significantly different from single treatment groups ($p < 0.01$).

(G and H) HEYA8 stably expressing control shRNA or TP53INP1 shRNA were injected intraperitoneally. Mice were treated with control antimiR or anti-miR569 starting on day 7 for 35 days. Tumors were isolated on day 42 and number of tumors (G) and tumor weight (H) calculated ($n = 10$ per group). Bars represent SEM. Significance was calculated with Student's t test.

See also Figure S7.